Pressure-induced Yb valence transition and magnetism in $YbMn_6Ge_{6-x}Sn_x$

L. Eichenberger,[1,*] M. François,[1] D. Malterre,[1] R. Sibille,[2] N. P. M. Casati,[3] L. Nataf,[4] F. Baudelet,[4,†] and T. Mazet[1]

[1]*Université de Lorraine, CNRS, IJL, F-54000 Nancy, France*

[2]*Laboratory for Neutron Scattering and Imaging, Paul Scherrer Institut, CH-5232 Villigen PSI, Switzerland*

[3]*Swiss Light Source, Paul Scherrer Institut, CH-5232 Villigen PSI, Switzerland*

[4]*Synchrotron SOLEIL, UR1 CNRS, Saint-Aubin-BP48, 91192 Gif-sur-Yvette, France*

(Received 22 March 2023; revised 12 May 2023; accepted 12 May 2023; published 24 May 2023)

We investigate the external pressure dependence of the crystal structure, Yb valence, and local magnetization in $YbMn_6Ge_{6-x}Sn_x$ using x-ray diffraction, x-ray absorption near edge spectroscopy (XANES), and x-ray magnetic circular dichroism (XMCD). The application of physical pressure results in a weakly anisotropic unit cell volume contraction without modifying the crystal structure. The external pressure allows crossing the Yb magnetic instability, which occurs for strongly hybridized Yb (valence ≈2.76), with a concomitant slope change in the valence-pressure curve. In the Ge-rich compounds, Yb local magnetism vanishes at very high pressure ($P \geqslant 39.8$ GPa) likely because of the simultaneous collapse of the Mn magnetism. The results underline similarities between external and chemical pressure increase, which favors trivalent and magnetic Yb. Some differences are observed in the Sn-rich compounds highlighting potential local pressure and/or electronic effects.

DOI: 10.1103/PhysRevB.107.205146

I. INTRODUCTION

In condensed-matter physics, Yb- or Ce-based intermetallics are relevant candidates to study quantum critical effects such as non-Fermi-liquid behavior or unconventional superconductivity [1,2]. These exotic phases have been mainly investigated in materials where the rare-earth-metal element is alloyed with nonmagnetic elements [1,3] and are often limited to very low temperature and trivalent rare earth metals [2,4]. In most cases, the physics of such systems can be understood based on the Doniach picture [5], where Kondo screening competes with Ruderman-Kittel-Kasuya-Yoshida (RKKY) exchange interactions. Their relative magnitude can be varied using nonthermal control parameters (chemical substitution, pressure, magnetic field) to cross the rare-earth-metal magnetic instability where quantum critical effects may manifest [1,2]. Other heavy fermion materials deviate from this behavior and are termed unconventional [6–9] with, in some cases, quantum critical effects completely detached from the rare-earth-metal magnetic instability [10–13]. In all these materials, Yb or Ce are alloyed with nonmagnetic elements and, for the sake of simplicity, we hereafter term them *standard* materials.

In $YbMn_6Ge_{6-x}Sn_x$ [14–19], the situation is rather different since the Mn sublattice, which orders magnetically near room temperature or above, interacts with intermediate valent Yb. The Mn($3d$)-Yb($4f$) exchange interaction is substantially stronger than $4f$-$4f$ RKKY interactions [20,21]. This results in unusually high magnetic ordering temperatures of intermediate valent Yb (up to $T_{Yb} \approx 125$ K) [17] and a shift of the magnetic instability toward strongly hybridized Yb (Yb valence $\upsilon \approx 2.77$ at the critical composition $x_c \approx 5.23$) [18]. This kind of heavy fermion systems also shows signatures of quantum criticality near x_c, with an enhancement of the effective mass of the charge carriers [19] and of the Yb valence and $4f$ magnetism [18]. This manifests by a marked peak in their composition dependence, in agreement with theories on unconventional quantum criticality which predict divergent valence and magnetic susceptibilities at the quantum critical point [22,23].

In $YbMn_6Ge_{6-x}Sn_x$, the hybridization between $4f$ and conduction electrons, thus the Yb valence υ, is altered by chemical pressure using the isoelectronic substitution of Sn for Ge. The Yb valence ranges from $\upsilon \approx 3$ for $x = 0.0$ down to $\upsilon \approx 2.6$ for $x = 6.0$ [18]. Chemical or external pressure variation may modify physical properties through various mechanisms as the contraction of interatomic distances (in turn changing the magnetic exchange interactions and/or rare-earth-metal valence) [7,24–26] or modifications of the electronic structure (increase of the bandwidth and depression of the electronic density of states at the Fermi level) [27,28]. In *standard* Yb-based heavy fermion materials, pressure increase promotes trivalent Yb and therefore Yb magnetism [7,24–26], due to the decrease of the $4f$-conduction electron hybridization, which alters the balance between Kondo effect (T_K) and the RKKY interaction (T_{RKKY}) [29]. Ce-based materials behave oppositely, with an increase of the hybridization and loss of magnetism upon pressure increase.

In the present work, we investigate the influence of external pressure change on the crystal structure, Yb valence, and magnetism in $YbMn_6Ge_{6-x}Sn_x$, using x-ray diffraction, Yb L_3 edge x-ray absorption near edge spectroscopy (XANES), and x-ray magnetic circular dichroism (XMCD). We compare the effect of physical pressure to chemical pressure. This work

*Corresponding author: lucas.eichenberger@univ-lorraine.fr

†Deceased.

is organized as follows: Section II provides the experimental details. The results are presented in Sec. III and discussed in Sec. IV before a short conclusion in Sec. V.

II. EXPERIMENTAL DETAILS

The polycrystalline $YbMn_6Ge_{6-x}Sn_x$ samples investigated here (and the two related Lu-based samples) were prepared from high-purity elements as described in Refs. [14,17]. These two papers also report on the crystal and magnetic properties determined by x-ray diffraction, DC magnetization, and neutron diffraction measurements. Due to limited beam time, only a few samples were investigate with x-ray diffraction experiments under external pressure. The experiments were carried out up to ≈ 10 GPa at room temperature using the synchrotron radiation delivered by the beam line MS-X04SA ($\lambda = 0.62$ Å) at the Swiss Light Source (SLS, Paul Scherrer Institute, Villigen, Switzerland) [30]. External pressure was applied using a diamond anvil cell with silicon oil as the pressure-transmitting medium. The pressure was evaluated from the variation of the quartz unit-cell parameters [31]. The x-ray diffraction patterns were analyzed by Le Bail refinements using the FULLPROF software [32].

The XANES and XMCD spectra at the Yb L_3 edge were recorded using the ODE beam line of the SOLEIL synchrotron (Saint-Aubin, France) [33]. The dichroism effect is given by the difference between the x-ray absorption intensities recorded under an applied field of 1.3 T aligned parallel and antiparallel to the beam while keeping constant the beam helicity. The experiments were carried out in the 5–300 K temperature range and under external pressure up to ≈ 50 GPa thanks to a diamond anvil cell with silicon oil as transmitting medium. The shift of the $R1$ fluorescence line of a ruby [34] was used to measure the pressure. Due to occasional failures of the high-pressure cell, some compositions were investigated in a more reduced pressure range.

III. EXPERIMENTAL RESULTS

A. X-ray diffraction under pressure

X-ray diffraction experiments under pressure were carried out on five $YbMn_6Ge_{6-x}Sn_x$ compositions ($x = 0.00$, 3.80, 4.25, 4.40, 5.80) as well as on two related Lu-based compounds (namely, $LuMn_6Ge_{1.8}Sn_{4.2}$ and $LuMn_6Sn_6$), the latter two with a stable $4f$ shell rare-earth-metal element serving as reference materials. Le Bail refinement of the data indicates that all compounds keep the $HfFe_6Ge_6$-type structure ($P6/mmm$), with one site for Mn, one site for Yb, and three sites for the p elements [14]. The cell volume contracts upon external pressure increase without structural transition up to the maximal applied pressure used of 10 GPa. Depending on composition, the volume contraction at 10 GPa lies between 7 and 10% of the ambient pressure unit cell volume V_0 [see Fig. 1(a)]. The contraction is slightly anisotropic since the ratio c/a increases with pressure [see inset of Fig. 1(a)]. By contrast, the ratio c/a decreases upon chemical pressure increase (i.e., upon decreasing the Sn content) [35]. This suggests that chemical and hydrostatic pressure variations do not have strictly the same effect. In $YbRh_2Si_2$, the ratio c/a also evolves dissimilarly depending on whether the contraction is due to hydrostatic pressure increase or to chemical pressure increase from Co for Rh substitution [7].

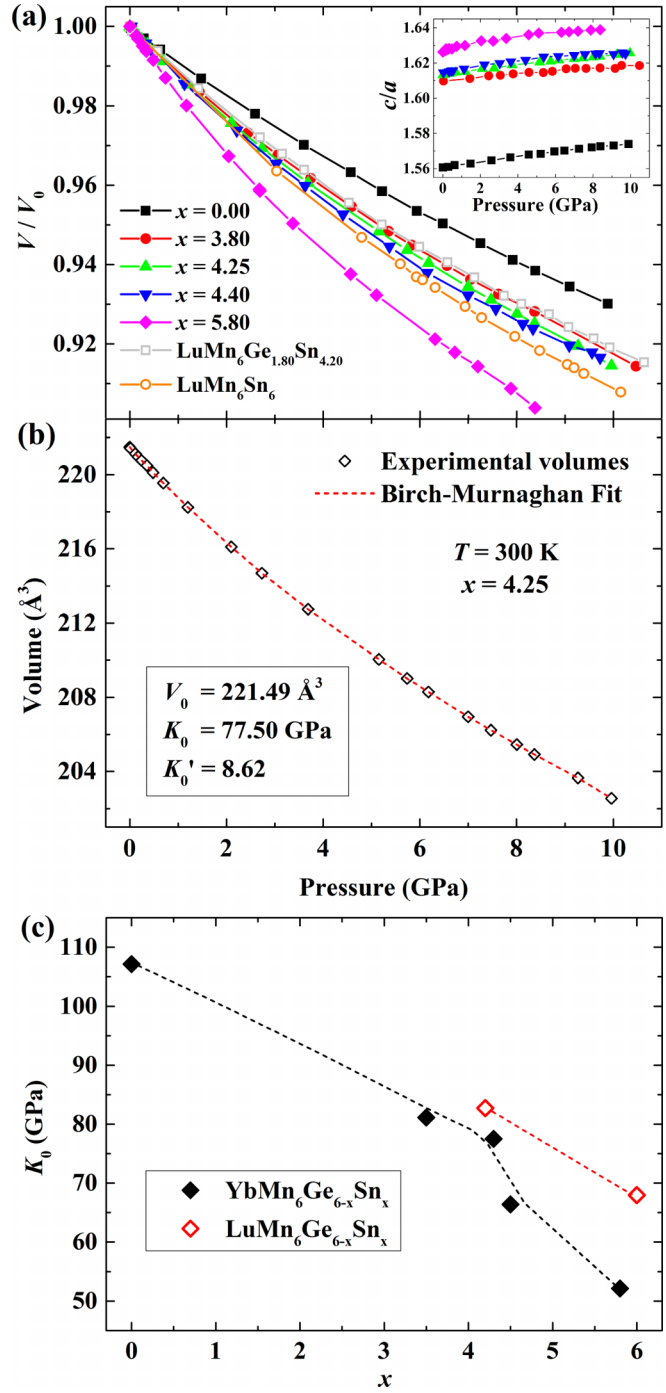

FIG. 1. (a) Pressure variation of the normalized unit cell volume V/V_0 (V_0 is the ambient pressure unit cell volume) in $YbMn_6Ge_{6-x}Sn_x$ and $LuMn_6Ge_{6-x}Sn_x$ at 300 K. The insert shows c/a variation for Yb-based alloys. (b) Fit to third-order Birch-Murnahgan's equation of state of $YbMn_6Ge_{1.75}Sn_{4.25}$. (c) Composition dependence of the bulk modulus K_0 in $YbMn_6Ge_{6-x}Sn_x$ and $LuMn_6Ge_{6-x}Sn_x$.

The bulk modulus K_0, which characterizes the compression behavior under hydrostatic pressure, was extracted from the data by fitting a third-order Birch-Murnahgan equation of

state [36]:

$$P = \frac{3}{2}K_0\left[\left(\frac{V_0}{V}\right)^{\frac{7}{3}} - \left(\frac{V_0}{V}\right)^{\frac{5}{3}}\right] \times \left[1 + \frac{3}{4}(K_0' - 4)\left[\left(\frac{V_0}{V}\right)^{\frac{2}{3}} - 1\right]\right],$$

where V_0, K_0, and K_0' are the ambient pressure volume, bulk modulus, and its pressure derivative, respectively. As an example, Fig. 1(b) shows the fit for $x = 4.25$.

In both the Yb and Lu series, K_0 decreases upon increasing the Sn content, indicating that compressing the alloys becomes easier [Fig. 1(c)]. This is most likely due to weaker chemical bonds with Sn than with Ge in such intermetallics [37,38]. In addition, our results reveal higher compressibility of compounds with intermediate valent Yb alloys [18] compared with the Lu-based compounds of similar tin content. This difference likely originates from the Yb $4f^{14}(spd)^2 \rightarrow 4f^{13}(spd)^2$ pressure induced gradual transition [25], absent in the stable $4f$ shell Lu-based counterparts. The compressibility gap between the Yb and Lu series increases with the Sn content due to the concomitant reduction of the Yb valence [18].

B. XANES

XANES measurements have been performed at 5 K on several $YbMn_6Ge_{6-x}Sn_x$ alloys ($3.80 \leqslant x \leqslant 5.80$) and also at 300 K for $x = 4.95$. The L_3-edge XANES spectra of $YbMn_6Ge_{0.2}Sn_{5.8}$ recorded at 5 K upon increasing hydrostatic pressure are shown in Fig. 2(a). A typical intermediate valent Yb L_3 edge XANES spectrum consists of two structures: a main peak at 8.948 keV and a shoulder at 8.941 keV, which correspond to transitions from the initial state to the final states of mainly $2p^5 4f^{13}$ (trivalent) and $2p^5 4f^{14}$ (divalent) character, respectively. As expected [7,24–26], increasing external pressure yields a spectral weight transfer from the Yb^{2+} component toward the Yb^{3+} one. The same is true for all compositions. The Yb valence υ is obtained by fitting the divalent and trivalent components as described in Refs. [18,39]. Figure 2(b) presents the pressure dependence of the Yb valence for the whole $YbMn_6Ge_{6-x}Sn_x$ series.

Above 10 GPa, Yb reaches the fully trivalent state in almost all compounds, except in the richest Sn compound ($x = 5.80$) which remains slightly below trivalency at the highest applied pressure ($\upsilon_{max} \sim 2.98$ at $P \sim 50$ GPa). This points will be further discussed in Sec. IV.

Three kinds of behavior can be distinguished depending on the Sn content. For $x \leqslant 4.65$, Yb is nearly trivalent at ambient pressure ($\upsilon > 2.95$) and Yb valence increases slowly and continuously with pressure ($\frac{\partial \upsilon}{\partial P} \approx 0.005\,\mathrm{GPa}^{-1}$) until saturation. For an intermediate composition ($x = 4.95$) the Yb valence increases sharply from the lowest pressures ($\frac{\partial \upsilon}{\partial P} \approx 0.02\,\mathrm{GPa}^{-1}$) to reach trivalency above 8 GPa. For this composition only, the pressure dependence was also measured at room temperature and is almost identical to that recorded at low temperature [open blue diamonds in Fig. 2(b)]. Finally, in the Sn-rich compounds ($x \geqslant 5.23$), Yb is farther from trivalency at ambient pressure ($\upsilon < 2.80$). The $\upsilon(P)$ curves starts with a plateau-like behavior at low pressure

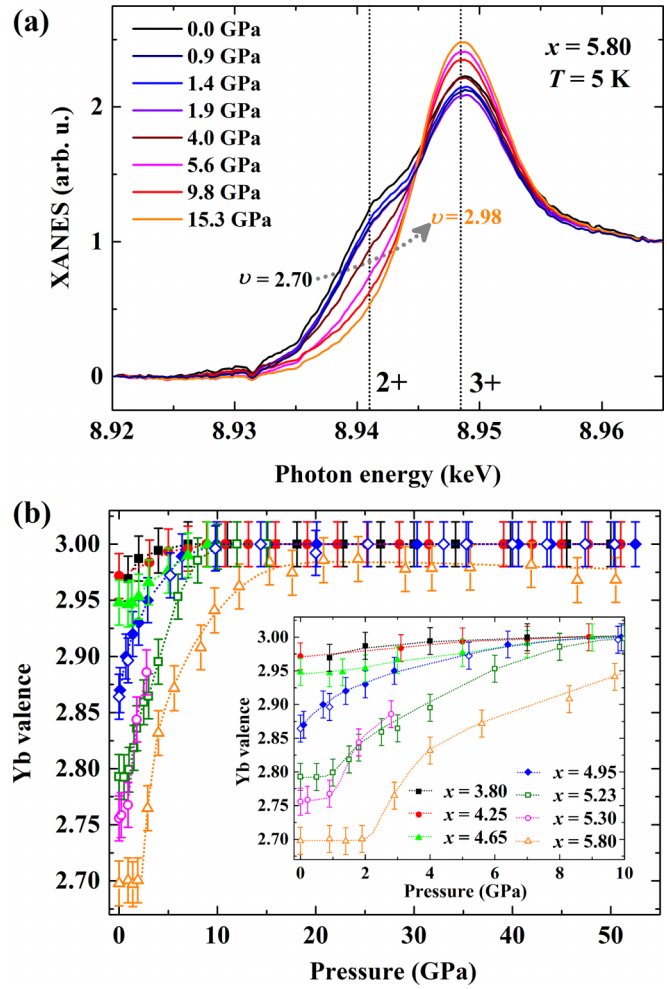

FIG. 2. (a) Yb L_3 XANES spectra of $YbMn_6Ge_{0.2}Sn_{5.8}$ at 5 K for different applied pressures. (b) Pressure dependence of the Yb valence at 5 K of $YbMn_6Ge_{6-x}Sn_x$ extracted from the XANES spectra. The inset shows an enlargement of the low-pressure region ($P <$ 10 GPa). Room-temperature data are also shown for $x = 4.95$ (open blue diamonds).

($\frac{\partial \upsilon}{\partial P} \approx 0\mathrm{GPa}^{-1}$), which extends with the Sn content. Beyond this plateau, the Yb valence strongly increases with pressure ($\frac{\partial \upsilon}{\partial P} \approx 0.03\,\mathrm{GPa}^{-1}$), as does the intermediate composition $x = 4.95$ at low pressure, before slowly reaching ($5.23 \leqslant x \leqslant 5.30$) or approaching ($x = 5.80$) the fully trivalent state above 10 GPa.

We now approximately evaluate the chemical pressure, to compare its influence with that of hydrostatic pressure, by combining the ambient pressure crystallographic data (see Refs. [14,17]) and data from x-ray diffraction under pressure (cf. Sec. III A). We proceed as follows. The richest Sn alloys ($x = 5.8$) with the larger cell volume is chosen as the zero of chemical pressure. We use the experimental $\upsilon(P)$ curve of $x = 5.8$ to locate the ambient pressure volumes of the other compounds with $x < 5.8$. For each composition, the corresponding pressure is taken as the chemical pressure [Fig. 3(a)]. For instance, for $x = 4.65$ the chemical pressure is estimated to be $P_{chem} = 4.1$ GPa.

Figure 3(b) shows the evolution of the Yb valence as a function of the total pressure ($P_{external} + P_{chem}$). The curves

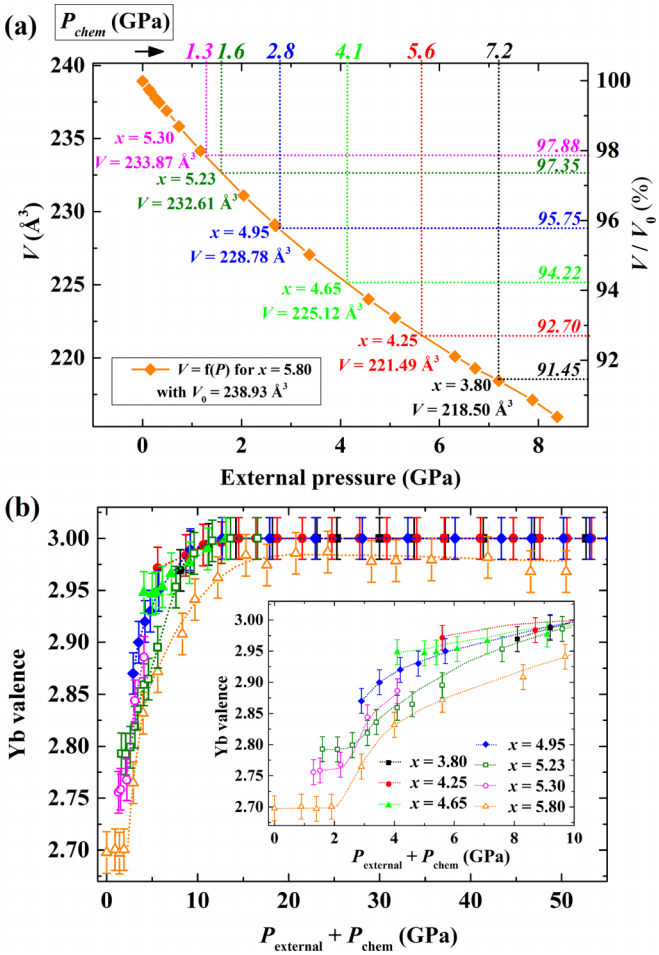

FIG. 3. (a) Estimation of the initial chemical pressure P_{chem} in $YbMn_6Ge_{6-x}Sn_x$. The pressure variation of the unit cell volume of the Sn-rich reference alloy $x = 5.80$ is taken from Fig. 1(a). Right scale shows the normalized unit cell volume, V_0 being the room-temperature lattice volume of $x = 5.80$. The room-temperature lattice volumes are also shown for all the measured compositions (data from Refs. [14,17]). (b) Yb valence at 5 K as a function of total pressure ($P_{external} + P_{chem}$) of $YbMn_6Ge_{6-x}Sn_x$, inset showing an enlargement of the low-pressure region ($P < 10$ GPa).

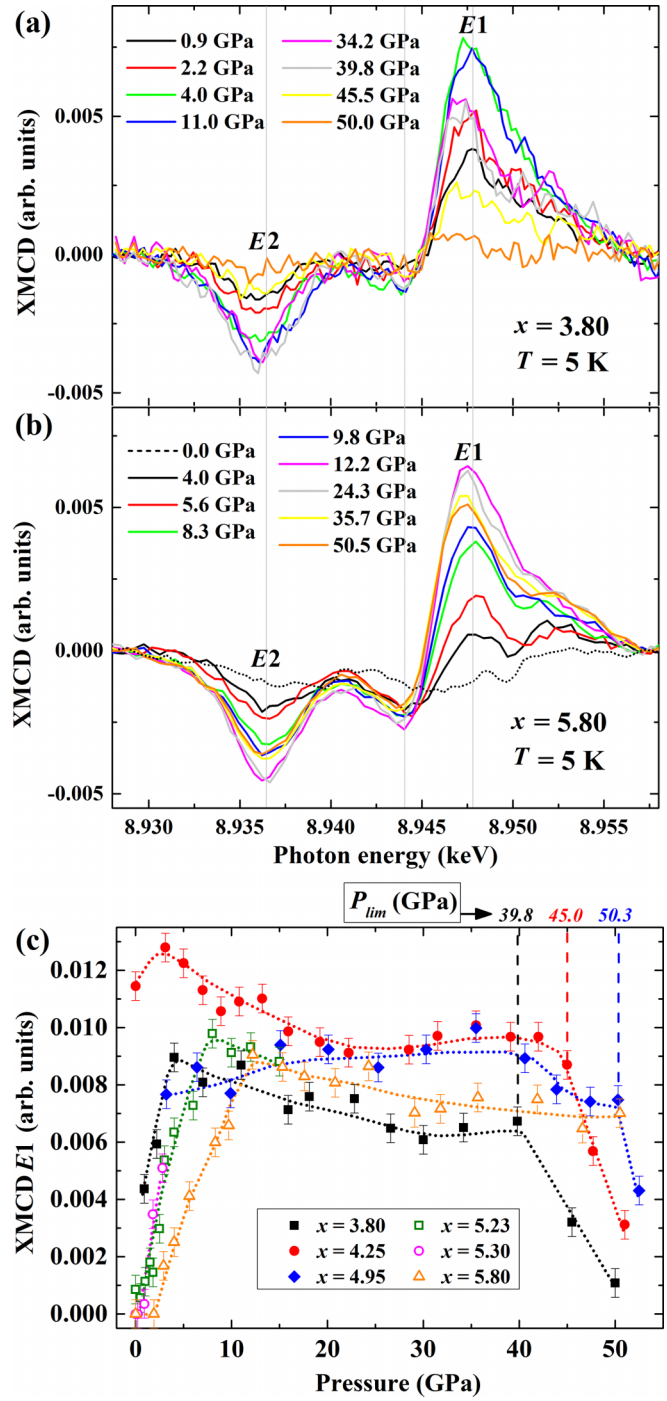

FIG. 4. (a) Yb L_3 XMCD spectra of $YbMn_6Ge_{2.20}Sn_{3.80}$ and (b) $YbMn_6Ge_{0.20}Sn_{5.80}$ at 5 K for different applied pressures. (c) Pressure dependence of the dipolar XMCD signal ($E1$) at 5 K in $YbMn_6Ge_{6-x}Sn_x$. P_{lim} indicates the pressure at which the $E1$ signal starts to strongly decrease.

were obtained by shifting of P_{chem} those shown in Fig. 2(b). Most of the data points are then scattered around an S-shaped curve. This indicates that external and chemical pressure are almost equivalent. The main differences are observed for the Sn-rich compounds ($x \geqslant 5.23$) for which the plateaus occur for unlike Yb valences. In addition, as mentioned above, the richest Sn alloys $x = 5.8$ does not reach the fully trivalent state at high pressure. This suggests that, in the Sn-rich region, hydrostatic pressure and isoelectronic Ge/Sn substitution are not strictly equivalent.

C. XMCD

The pressure-dependent Yb L_3 edge XMCD measurements were used to probe the local magnetism of Yb at 5 K. This is a qualitative study since sum rules do not apply to the L_3 edge of rare-earth metals [40]. A complete description of the XMCD spectra in $YbMn_6Ge_{6-x}Sn_x$ can be found in Ref. [18]. They comprise three contributions [Fig. 4(a)]: one negative peak at $E \approx 8.937$ keV resulting from quadrupolar transitions ($2p \rightarrow 4f$) and two other ones of dipolar origin ($2p \rightarrow 5d$) at higher energy ($E \approx 8.944$ keV and $E \approx 8.948$ keV). The weak negative peak at $E \approx 8.944$ keV is due to the hybridization of the $5d$ states of Yb with the self-polarized $3d$ states of Mn. The large positive peak at $E \approx 8.948$ keV is

ascribed to local exchange interaction with the $4f$ spin. Thus, Yb $4f$ magnetism yields the quadrupolar ($E2$) and the large dipolar contributions ($E1$) while the weak negative peak at $E\approx 8.944$ keV remains present and almost constant as long as the Mn sublattice is ordered. Thereafter, we only follow the pressure dependence of the main $E1$ contribution at 5 K (the evolution of the $E2$ contribution being very similar). The pressure dependence of the XMCD spectra of $x = 3.8$ and 5.8 is shown in Figs. 4(a) and 4(b), respectively. The pressure dependence of $E1$ is plotted in Fig. 4(c) for all investigated compositions.

External pressure induces an increase of the Yb valence (cf. Sec. III B) and thus strengthens Yb $4f$ magnetism. This is evidenced by the strong increase of the $E1$ contribution under moderate external pressure ($P < 10$ GPa) [Fig. 4(c)]. For the Sn-rich alloys ($x = 5.30$ and 5.80), within which Yb is nonmagnetic at ambient pressure [18], the $E1$ and $E2$ contributions become nonzero beyond a composition-dependent critical pressure, proving the onset of $4f$ magnetism. After the initial growth, the XMCD signal intensity keeps almost constant up to the highest pressure of the measurements ($\approx$50 GPa) except for the three poorer Sn alloys ($x = 3.80$, 4.25, and 4.95) for which a sharp decrease of the XMCD signal is observed beyond a composition-dependent pressure $P_{\rm lim}$. This indicates that, although Yb is fully trivalent, it loses its magnetic character under high enough hydrostatic pressure.

IV. DISCUSSION

Our study shows that increasing the hydrostatic pressure or the chemical pressure through isoelectronic Ge for Sn substitution has globally similar effect: It yields an increase of the Yb valence and promotes Yb $4f$ magnetism. However, besides the dissimilar influence of external and chemical pressure on the ratio c/a, some other differences manifest in the Sn-rich alloys ($x \geqslant 5.23$).

When $x \geqslant 5.23$, the Yb valence is found insensitive to low applied pressure (<2 GPa) whereas the ambient pressure Yb valence evolves gradually with composition $5.23 \leqslant x \leqslant 5.80$ [18], although in both cases the volume contraction is of comparable magnitude [a few percent; see Fig. 3(a)]. We can identify two possible origins for this discrepancy. First, the chemical pressure acts locally; the Ge for Sn substitution takes place on the metalloid $2d$ site [17] which is coplanar of Yb and in its first coordination shell. As a result, weak changes in the Ge/Sn content yields significant modification of the interatomic distances between Yb and its first neighbors. By contrast, hydrostatic pressure acts on the whole lattice, making it less influential on local interatomic distances around Yb. Additional x-ray diffraction experiments performed to allow Rietveld refinements should help to compare the effects of chemical and external pressure by following interatomic distances modifications. The second possible origin for the differences between chemical and physical pressure behaviors invokes electronic effects. Though Ge and Sn are isovalent, the dissimilarity between the Ge $4s4p$ and the less bound Sn $5s5p$ valence states could yield different electronic structures near the Fermi level that influence the Yb valence. For instance, in the magnetocaloric $Gd_5(Si_xGe_{1-x})_4$ alloys, the influence of Ge for Si substitution arises predominantly from an electronic effect rather than from volume variation [41].

A difference in the electronic structure near the Fermi level might also explain the singular high-pressure behavior of $x = 5.8$—the sole alloy for which Yb does not reach trivalency and even tends to reduce under high hydrostatic pressure. Several examples reported in the literature [27,42,43] show that a saturation or a decrease of the Yb valence may be observed despite the concomitant reduction of the lattice parameters. This unusual decrease of the Yb valence with pressure cannot be explained with conventional $c - f$ hybridization. It might arise from the competition between two ways of coupling f-electrons and the lattice, as explained in Ref. [44], resulting in a pressure-induced enhancement of the Kondo effect due to an increase of both the hybridization strength and the width of the conduction band [43,44].

A last remark about the pressure dependence of the Yb valence involves intermediate compositions, in particular $x = 4.95$, whose Yb valence shows a strong sensitivity to low applied pressure variation [Fig. 3(a)], thus to weak interatomic distance changes ($\approx$1%) comparable to those due to thermal contraction. As suggested in Refs. [15,16], this strong sensitivity could participate in the unusual increase of the Yb valence observed upon cooling for intermediate $YbMn_6Ge_{6-x}Sn_x$ compositions (ca. $4 < x < 5$), in addition to the effect due to the increasing exchange field.

At ambient pressure, the alloy with $x = 5.23$ ($\upsilon \approx 2.77$) is the richest Sn alloy whose low-temperature XMCD spectrum shows trace of $4f$ magnetism [18]. It is thus located close to the Yb magnetic instability and the associated quantum criticality, while Yb is nonmagnetic in richer Sn alloys. Increasing the external pressure on the two alloys with initially nonmagnetic Yb ($x = 5.30$ and 5.80) allows stabilizing $4f$ magnetism [see Figs. 4(a) and 4(b)], as observed in many *standard* Yb heavy fermion materials close to trivalency [24,45]. The low-pressure ($P < 4$ GPa) variation of the Yb valence and XMCD $E1$ contribution are shown together in Fig. 5 for these two alloys ($x = 5.30$ and 5.80). Both the Yb valence υ and the $E1$ contribution evolve similarly. We first note that the lower pressure point for which $4f$ magnetism is detected in the XMCD spectra corresponds to a Yb valence of $\upsilon \approx 2.76$, almost identical to that reported at ambient pressure, but considerably lower than the valence at which Yb magnetism may appear in *standard* materials where Yb is alloyed with nonmagnetic elements. We further observe that the XMCD $E1$ contribution remains zero as long as the Yb valence keeps independent of pressure, and $4f$ magnetism appears when the Yb valence starts to grow (i.e., when there is a marked slope change in the $\upsilon(P)$ curves), that is near $\approx$1 GPa and 2 GPa for, respectively, $x = 5.30$ and 5.80. Slope changes in the pressure dependence of the Yb valence—but generally corresponding to a slope reduction—are often considered as a marker of quantum criticality in *standard* heavy fermion materials [45–48].

In previous works [18,19], we identified the peak near $x_c \approx 5.23$ (whose base width is estimated to be $\Delta x \approx 0.05$ from the data in Ref. [18]) in the composition dependence of the Yb valence, XMCD intensity, and electronic specific heat coefficient as signs of quantum criticality. We do not observe

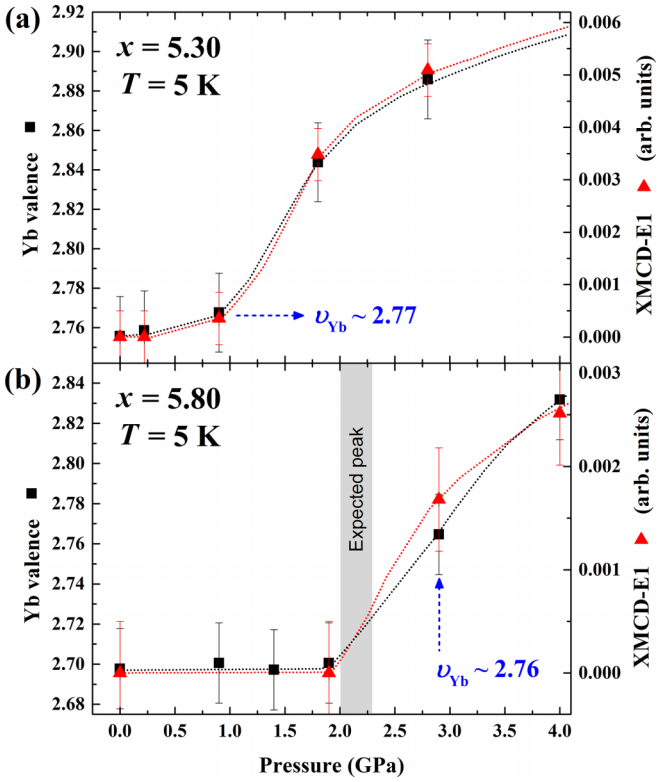

FIG. 5. Pressure dependence ($P < 4$ GPa) of the Yb valence (black squares, left scale) and of the Yb $E1$ XMCD contribution (red triangles, right scale) at 5 K for (a) $YbMn_6Ge_{0.70}Sn_{5.30}$ and (b) $YbMn_6Ge_{0.20}Sn_{5.80}$. The shaded area shows the pressure domain where a peak in the pressure dependence of the Yb valence and XMCD signal is expected for $x = 5.8$ [18] (see text).

such a peak in the pressure dependence of the Yb valence and $E1$ XMCD [Figs. 2(b), 4(c), and 5]. Based on the data in Fig. 3(a), the peak width is estimated to be $\Delta P \approx 0.2$ GPa and located near $P \approx 2$ GPa for $x = 5.80$. However, most of the pressure-dependent measurements have been performed before we realized the existence of that divergence, such that the pressure steps we used (at least ≈0.5 to 1 GPa) were too large and the peak might have been missed [see the shaded area in Fig. 5(b)]. Further, we used silicon oil as the pressure-transmitting medium, resulting in pressure gradients across the sample chamber (≈0.25 GPa for 2 GPa $< P <$ 10 GPa) [50] that may hinder the detection of the divergence.

As noticed in Sec. III C, the $E1$ XMCD intensity dramatically decreases at high pressure in the three richest Ge investigated alloys ($x = 3.80$, 4.25, and 4.95) despite Yb is then fully trivalent [Fig. 4(c)]. The pressure at which the XMCD signal starts to fall off (P_{lim}) reduces upon increasing the Ge content, that is upon reducing the lattice parameters. Since this disappearance of $4f$ Yb magnetism seems unrelated to Yb valence fluctuations, we propose it may come from the collapse of the Mn magnetic moment, in agreement with the almost flat XMCD signal of the $x = 5.8$ composition at ≈50 GPa [see Fig. 4(a)]. Since the unusually high temperature magnetic ordering of Yb is thought to be due to the strong Mn-Yb exchange interaction [15–18], the collapse of the Mn magnetism yields in turn the destabilization of the Yb sublattice magnetic order. The breakdown of Mn magnetism can be understood based on simple arguments in the framework of the Stoner's model [49]. At sufficiently high pressure [above P_{lim} in Fig. 4(c)], the Mn-Mn distances are considerably reduced. The electronic bandwidth widens such that the density of states at the Fermi level becomes too low for the Stoner criterion to be satisfied, and in turn Mn loses its magnetic moment. Since the Mn-Mn distances shorten upon Ge for Sn substitution, P_{lim} tends to decrease with the Ge content while the lost of Yb magnetism is not observed in the Sn-rich compositions.

V. CONCLUSION

We have investigated the pressure dependence of the crystal structure, Yb valence and Yb $4f$ magnetism in $YbMn_6Ge_{6-x}Sn_x$ using, respectively, x-ray diffraction, XANES, and XMCD measurements at the Yb L_3 edge. Our results show that external or chemical pressure have overall the same influence, as often observed in heavy fermion materials: A pressure increase promotes Yb trivalency and strengthens Yb magnetism. Some differences were observed, mainly in the Sn-rich region, that we tentatively ascribed to the local nature of chemical pressure changes and/or to different binding and spatial extent of the valence electrons of isoelectronic Ge and Sn.

Once plotted as a function of total pressure (= external + chemical), the Yb valence follows an S-shaped curve. At low external pressure, for alloys with initially nonmagnetic Yb, the Yb valence is insensitive to external pressure change, while chemical pressure variation yields a gradual change of the valence throughout the series. Upon further total pressure increase, the Yb valence changes quickly with pressure before slowing down when trivalency is approached. The strong slope increase at low pressure corresponds to the Yb magnetic instability, i.e., to the appearance of Yb magnetism. This instability occurs at nearly the same valence ($\upsilon \approx 2.76$) as for changes of the Sn content at ambient pressure. The pressure-induced magnetic instability might be connected to quantum critical effects, but we did not observe the singularity in the Yb valence and XMCD signal previously found at ambient pressure. This is likely due to the sparse pressure points available due to limited beam-time availability. We proposed that the fall of the XMCD signal at elevated pressure observed in the Ge-rich alloys might arise from the collapse of Mn magnetism due to $3d$-band broadening.

Further experiments may be helpful for a better understanding of these atypical series and to verify some of our assumptions. For instance, x-ray data allowing Rietveld refinements to detect difference in interatomic distances variation upon changing chemical or external pressure as well as pressure-dependent XMCD measurements at the Mn K edge to verify the collapse of Mn magnetism.

ACKNOWLEDGMENTS

We acknowledge the Paul Scherrer Institute, Villigen, Switzerland (Exp. No. 20131006) and the French Synchrotron facility SOLEIL, Saint-Aubin, France (Exps. No. 20130845, No. 20140775, and No. 20170707) for the allocated beam time.

[1] H. V. Löhneysen, A. Rosch, M. Vojta, and P. Wölfle, Rev. Mod. Phys. **79**, 1015 (2007).

[2] For a review, see P. Coleman, in *Handbook of Magnetism and Advanced Magnetic Materials*, edited by H. Kronmüller and S. Parkin (Wiley, New York, 2007), and references therein.

[3] E. Morosan, D. Natelson, A. H. Nevidomskyy, and Q. Si, Adv. Mater. **24**, 4896 (2012).

[4] E. Bauer, R. Hauser, L. Keller, P. Fischer, O. Trovarelli, J. G. Sereni, J. J. Rieger, and G. R. Stewart, Phys. Rev. B **56**, 711 (1997).

[5] S. Doniach, Physica B + C (Amsterdam) **91**, 231 (1977).

[6] E. D. Mun, S. L. Budko, C. Martin, H. Kim, M. A. Tanatar, J.-H. Park, T. Murphy, G. M. Schmiedeshoff, N. Dilley, R. Prozorov, and P. C. Canfield, Phys. Rev. B **87**, 075120 (2013).

[7] C. Klingner, C. Krellner, M. Brando, C. Geibel, F. Steglich, D. V. Vyalikh, K. Kummer, S. Danzenbächer, S. L. Molodtsov, C. Laubschat, T. Kinoshita, Y. Kato, and T. Muro, Phys. Rev. B **83**, 144405 (2011).

[8] H. Nakai, T. Ebihara, S. Tsutsui, M. Mizumaki, N. Kawamura, S. Michimura, T. Inami, T. Nakamura, A. Kondo, K. Kindo, and Y. H. Matsuda, J. Phys. Soc. Jpn. **82**, 124712 (2013).

[9] Y. Luo, X. Lu, A. P. Dioguardi, P. S. F. Rosa, E. D. Bauer, Q. Si, and J. D. Thompson, npj Quantum Mater. **3**, 6 (2018).

[10] S. Nakatsuji, K. Kuga, Y. Machida, T. Tayama, T. Sakakibara, Y. Karaki, H. Ishimoto, S. Yonezawa, Y. Maeno, E. Pearson, G. G. Lonzarich, L. Balicas, H. Lee, and Z. Fisk, Nat. Phys. **4**, 603 (2008).

[11] M. Okawa, M. Matsunami, K. Ishizaka, R. Eguchi, M. Taguchi, A. Chainani, Y. Takata, M. Yabashi, K. Tamasaku, Y. Nishino, T. Ishikawa, K. Kuga, N. Horie, S. Nakatsuji, and S. Shin, Phys. Rev. Lett. **104**, 247201 (2010).

[12] T. Tomita, K. Kuga, Y. Uwatoko, P. Coleman, and S. Nakatsuji, Science **349**, 506 (2015).

[13] K. Kuga, Y. Matsumoto, M. Okawa, S. Suzuki, T. Tomita, K. Sone, Y. Shimura, T. Sakakibara, D. Nishio-Hamane, Y. Karaki, Y. Takata, M. Matsunami, R. Eguchi, M. Taguchi, A. Chainani, S. Shin, K. Tamasaku, Y. Nishino, M. Yabashi, T. Ishikawa *et al.*, Sci. Adv. **4**, eaao3547 (2018).

[14] T. Mazet, H. Ihou-Mouko, D. H. Ryan, C. J. Voyer, J. M. Cadogan, and B. Malaman, J. Phys.: Condens. Matter **22**, 116005 (2010).

[15] T. Mazet, D. Malterre, M. François, C. Dallera, M. Grioni, and G. Monaco, Phys. Rev. Lett. **111**, 096402 (2013).

[16] T. Mazet, D. Malterre, M. François, L. Eichenberger, M. Grioni, C. Dallera, and G. Monaco, Phys. Rev. B **92**, 075105 (2015).

[17] L. Eichenberger, D. Malterre, B. Malaman, and T. Mazet, Phys. Rev. B **96**, 155129 (2017).

[18] L. Eichenberger, A. Magnette, D. Malterre, R. Sibille, F. Baudelet, L. Nataf, and T. Mazet, Phys. Rev. B **101**, 020408(R) (2020).

[19] P. Haraux, L. Eichenberger, L. V. B. Diop, and T. Mazet, Solid State Commun. **341**, 114551 (2022).

[20] M. S. S. Brooks, L. Nordström, and B. Johansson, J. Phys.: Condens. Matter **3**, 2357 (1991).

[21] P. Tils, M. Loewenhaupt, K. H. J. Buschow, and R. S. Eccleston, J. Magn. Magn. Mater. **210**, 196 (2000).

[22] S. Watanabe and K. Miyake, Jpn. J. Appl. Phys. **56**, 05FA01 (2017).

[23] J. H. Pixley, S. Kirchner, and K. Ingersent, and Q. Si, Phys. Rev. Lett. **109**, 086403 (2012).

[24] J. Plessel, M. M. Abd-Elmeguid, J. P. Sanchez, G. Knebel, C. Geibel, O. Trovarelli, and F. Steglich, Phys. Rev. B **67**, 180403(R) (2003).

[25] G. N. Chesnut and Y. K. Vohra, Phys. Rev. Lett. **82**, 1712 (1999).

[26] H. Winkelmann, M. M. Abd-Elmeguid, H. Micklitz, J. P. Sanchez, P. Vulliet, K. Alami-Yadri, and D. Jaccard, Phys. Rev. B **60**, 3324 (1999).

[27] T. Watanuki, D. Kawana, A. Machida, and A. P. Tsai, Phys. Rev. B **84**, 054207 (2011).

[28] K. Lin, Q. Li, R. Yu, J. Chen, J. P. Attfield, and X. Xing, Chem. Soc. Rev. **51**, 5351 (2022).

[29] J. D. Thompson and J. L. Lawrence, in *Handbook on the Physics and Chemistry of Rare Earths*, edited by K. A. Gschneidner Jr., L. Eyring, G. H. Lander, and C. Choppin (North-Holland, Amsterdam, 1994), Vol. 19, p. 383.

[30] F. Gozzo, B. Schmitt, T. Bortolamedi, C. Giannini, A. Guagliardi, M. Lange, D. Meister, D. Maden, P. Willmott, and B. D. Patterson, J. Alloys Compd. **362**, 206 (2004).

[31] R. J. Angel, D. R. Allan, R. Miletich, and L. W. Finger, J. Appl. Crystallogr. **30**, 461 (1997).

[32] J. Rodríguez-Carvajal, Phys. B: Condens. Matter **192**, 55 (1993).

[33] F. Baudelet, L. Nataf, and R. Torchio, High Press. Res. **31**, 136 (2011).

[34] K. Syassen, High Press. Res. **28**, 75 (2008).

[35] L. Eichenberger, Ph.D. thesis, Université de Lorraine, Lorraine, France, 2015, https://hal.univ-lorraine.fr/tel-01754537.

[36] F. Birch, Phys. Rev. **71**, 809 (1947).

[37] T. Mazet, J. Tobola, G. Venturini, and B. Malaman, Phys. Rev. B **65**, 104406 (2002).

[38] T. Mazet, J. Tobola, and B. Malaman, Eur. Phys. J. B **34**, 131 (2003).

[39] L. Eichenberger, G. Venturini, B. Malaman, L. Nataf, F. Baudelet, and T. Mazet, J. Alloys Compd. **695**, 286 (2017).

[40] P. Carra, B. T. Thole, M. Altarelli, and X. Wang, Phys. Rev. Lett. **70**, 694 (1993).

[41] Y. C. Tseng, D. Paudyal, Y. Mudryk, V. K. Pecharsky, K. A. Gschneidner Jr., and D. Haskel, Phys. Rev. B **88**, 054428 (2013).

[42] C. Dallera, E. Annese, J. P. Rueff, A. Palenzona, G. Vanko, L. Braicovich, A. Shukla, and M. Grioni, Phys. Rev. B **68**, 245114 (2003).

[43] H. Yamaoka, N. Tsujii, M. T. Suzuki, Y. Yamamoto, I. Jarrige, H. Sato, J.-F. Lin, T. Mito, J. Mizuki, H. Sakurai, O. Sakai, N. Hiraoka, H. Ishii, K.-D. Tsuei, M. Giovannini, and E. Bauer, Sci. Rep. **7**, 5846 (2017).

[44] A. V. Goltsev and M. M. Abd-Elmeguid, J. Phys.: Condens. Matter **17**, S813 (2005).

[45] A. Fernandez-Pañella, D. Braithwaite, B. Salce, G. Lapertot, and J. Flouquet, Phys. Rev. B **84**, 134416 (2011).

[46] H. Yamaoka, N. Tsujii, Y. Utsumi, H. Sato, I. Jarrige, Y. Yamamoto, J.-F. Lin, N. Hiraoka, H. Ishii, K.-D. Tsuei, and J. Mizuki, Phys. Rev. B **87**, 205120 (2013).

[47] H. Yamaoka, I. Jarrige, N. Tsujii, J.-F. Lin, N. Hiraoka, H. Ishii, and K.-D. Tsuei, Phys. Rev. B **82**, 035111 (2010).

[48] H. Sato, H. Yamaoka, Y. Utsumi, H. Nagata, M. A. Avila, R. A. Ribeiro, K. Umeo, T. Takabatake, Y. Zekko, J. Mizuki, J.-F. Lin, N. Hiraoka, H. Ishii, K.-D. Tsuei, H. Namatame, and M. Taniguchi, Phys. Rev. B **89**, 045112 (2014).

[49] E. C. Stoner, Proc. R. Soc. London, Ser. A **165**, 372 (1938).

[50] S. Klotz, J. C. Chervin, P. Munsch, and G. Le Marchand, J. Phys. D. Appl. Phys. **42**, 075413 (2009).